Electronic band structure of GaAs sawtooth-doping superlattices

J. M. Ferreyra* and C. R. Proetto
Centro Atómico Bariloche, 8400 San Carlos de Bariloche, Río Negro, Argentina
(Received 16 April 1990)

We report simple calculations (of the Kronig-Penney type) concerning the band structure and charge distribution of GaAs sawtooth-doping superlattices as a function of period and doping concentration. We have obtained, within the effective-mass approximation, analytic expressions for the subband energy levels and envelope wave functions of the system.

I. INTRODUCTION

In their original proposal in 1970,[1] Esaki and Tsu envisioned a one-dimensional (1D) periodic potential produced by a periodic variation of either impurities (doping superlattices) or alloy composition (compositional superlattices) in semiconductors, with a period shorter than the electron mean free path.

The introduction of the superlattice potential perturbs the host-semiconductor band structure in such a way as to give rise to narrow subbands separated by forbidden regions, or minigaps.

The idea of tailored new materials has attracted numerous scientists since then, with almost exclusive emphasis on compositional superlattices;[2] this type of structure allows an unambiguous observation of quantum-confined interband transitions.[3] Kronig-Penney models have been applied to study its quantum-confined energy subbands and wave functions.[4–9]

On the other hand, only very recently has it been possible to observe clearly size quantization in doping superlattices.[10–13] In their original work,[1] Esaki and Tsu proposed a homogeneous alternating n- and p-type doping. However, the solubility limit of impurities opposes a strong modulation of the superlattice potential on a short length scale (for a review on early work in doping superlattices, see Ref. 14).

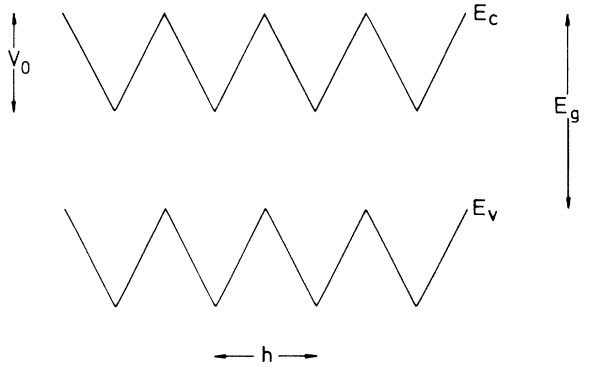

FIG. 1. Electronic band diagram of a sawtooth-doping superlattice. $E_c(E_v)$ is the energy corresponding to the bottom (top) of the conduction (valence) band of GaAs, E_g the bulk gap, and V_0 the band-edge modulation.

This problem has been overcome recently with the use of a δ-doping technique,[15] which allows one to localize impurity atoms on a lattice-constant length scale and to exceed locally the solubility limit of Si and Be in GaAs. A sawtooth-shaped band diagram is obtained as a consequence (see Fig. 1).

It should be pointed out that already in 1972, Döhler[16] made the first theoretical proposal on the interesting properties of these δ-doped superlattices.

Besides size quantization, very recently also excitonic effects in sawtooth-doping superlattices have been studied experimentally[10] and theoretically.[17]

It is the purpose of this work to report on our Kronig-Penney-type calculations of the band structure and charge distribution of sawtooth-doping superlattices. We have obtained, within the effective-mass approximation, analytic expressions for the subband energy levels and envelope wave functions of the system. For the particular case of band-edge energies, and as a consequence of the definite parity of the envelope wave functions, the general expressions for the subband energies and wave functions simplify considerably.

In Sec. II both the general case, valid for any energy, and the particular case of band-edge energies will be developed and compared. In Sec. III the results of Sec. II will be applied to the calculation of the band structure and charge distribution of GaAs sawtooth-doping superlattice. This application will then be discussed.

II. THEORY

We choose the z direction as the superlattice direction. Within the effective-mass approximation, the wave function corresponding to the particle [electron, heavy hole (hh), light hole (lh)] motion in the x-y plane is given by a simple plane wave.

The Schrödinger equation for motion in the z direction is

$$\left[-\frac{\hbar^2}{2m^*}\frac{d^2}{dz^2}+V(z)\right]\psi_{nk_z}(z)=E_n(k_z)\psi_{nk_z}(z)\ , \qquad (1)$$

m^* being the particle effective mass, and $\psi_{nk_z}(z)$ the envelope particle wave function corresponding to subband index n and wave vector k_z with eigenvalue $E_n(k_z)$.

In Eq. (1), $V(z)$ is the sawtooth-like potential of Fig. 1; for electrons it is given by

$$V(z)=eF\sum_{l=-\infty}^{\infty}|z-lh|\Theta((h/2)^2-(z-lh)^2)\ , \tag{2}$$

where $\Theta(x)$ is the unit-step function and h the superlattice period. A similar expression holds for the heavy and light holes, with z replaced by $z-h/2$ (see Fig. 1). Finally, the potential modulation V_0 is related to the two-dimensional δ-doping concentration N^{2D} according to

$$V_0=eFh/2=\pi e^2hN^{2D}/\epsilon\ , \tag{3}$$

where F is the built-in electric field in the superlattice, given by $F=2\pi eN^{2D}/\epsilon$, and ϵ is the dielectric constant of GaAs.

In the interval $0\le z\le h/2$, Eq. (1) for electrons reduces to

$$\left[-\frac{\hbar^2}{2m^*}\frac{d^2}{dz^2}+eFz\right]\psi^r_{nk_z}(z)=E_n(k_z)\psi^r_{nk_z}(z)\ , \tag{4}$$

whose exact solution is given by

$$\psi^r_{nk_z}(z)=a\ \mathrm{Ai}[-\beta(\alpha-z)]+b\ \mathrm{Bi}[-\beta(\alpha-z)]\ , \tag{5}$$

where Ai and Bi are Airy functions,[18] a,b are constants, and α,β are defined as follows:

$$\alpha=\frac{E_n(k_z)}{eF}\ ,\quad \beta=\left[\frac{2m^*eF}{\hbar^2}\right]^{1/3}\ . \tag{6}$$

For the sake of simplicity in the notation, we have omitted the dependence of the parameter α on band index n and wave vector k_z.

A similar analysis produces the solution in the left half of the well ($-h/2\le z\le 0$),

$$\psi^l_{nk_z}(z)=c\ \mathrm{Ai}[-\beta(\alpha+z)]+d\ \mathrm{Bi}[-\beta(\alpha+z)]\ , \tag{7}$$

where again c and d are constants to be determined.

In order to obtain the eigenvalue equation, we must impose on wave functions (5) and (7) the boundary conditions of continuity of the wave function and its derivative at $z=0$ and $h/2$,

$$\psi^r_{nk_z}(z=0)=\psi^l_{nk_z}(z=0)\ , \tag{8a}$$

$$\psi'^r_{nk_z}(z=0)=\psi'^l_{nk_z}(z=0)\ , \tag{8b}$$

$$\psi^r_{nk_z}(z=h/2)=e^{ik_zh}\psi^l_{nk_z}(z=-h/2)\ , \tag{8c}$$

$$\psi'^r_{nk_z}(z=h/2)=e^{ik_zh}\psi'^l_{nk_z}(z=-h/2)\ , \tag{8d}$$

where the last two equations follow from Bloch's theorem.[19] Note that, as pointed out in Ref. 11, unlike compositional superlattices, in doping superlattices the effective mass of the particles is the same everywhere and therefore it does not affect the boundary conditions. The primes in Eqs. (8b) and (8d) represent the derivative with respect to the whole argument (not to z).

Applying the condition that a, b, c, and d should not be zero simultaneously, we obtain

$$\det\begin{vmatrix} A_1 & B_1 & -A_1 & -B_1 \\ A_1' & B_1' & A_1' & B_1' \\ A_2 & B_2 & -e^{ik_zh}A_2 & -e^{ik_zh}B_2 \\ A_2' & B_2' & e^{ik_zh}A_2' & e^{ik_zh}B_2' \end{vmatrix}=0\ , \tag{9}$$

where $A_1=\mathrm{Ai}(-\alpha\beta)$, $B_1=\mathrm{Bi}(-\alpha\beta)$, $A_2=\mathrm{Ai}[-\beta(\alpha-h/2)]$, and $B_2=\mathrm{Bi}[-\beta(\alpha-h/2)]$.

Expanding the determinant in Eq. (9) and using the Wronskian relation satisfied by the Airy functions,[18]

$$\mathrm{Ai}(z)\mathrm{Bi}'(z)-\mathrm{Ai}'(z)\mathrm{Bi}(z)=1/\pi\ , \tag{10}$$

we find the eigenvalue equation

$$\cos(k_zh)=-\pi^2[(B_1A_2-B_2A_1)(A_2'B_1'-A_1'B_2')+(A_1B_2'-A_2'B_1)(A_1'B_2-A_2B_1')]\ , \tag{11}$$

a result that already was obtained in Refs. 11 and 13.

From Eq. (11) the dispersion relation $E_n(k_z)$ versus k_z can be readily obtained. We have determined—in Appendix A—the corresponding eigenfunctions, using Eqs. (5) and (7) and the system (8a)–(8d). We show in Appendix B that (11) reproduces, in the limit $h\to\infty$, the spectrum of a particle in a triangular potential, as it should.

Even though we have obtained analytical expressions for the eigenvalue equation and wave functions, the resulting equations are rather complicated.

Simpler results can be obtained, however, if the analysis is limited to the edge energies of each band. The band-edge energies and corresponding envelope wave functions can be useful to analyze the superlattice properties. A similar analysis has been carried out for the case of compositional $GaAs/Al_xGa_{1-x}As$ superlattices in Ref. 9.

Note first that the wave functions corresponding to the edge energies must have definite parity. This follows from Bloch's theorem, together with the dispersion relation (11). According to this last equation, the left-hand side can take the maximum (minimum) value of $+1$ (-1) when $k_{\mathrm{edge}}=0$ ($k_{\mathrm{edge}}=\pm\pi/h$). This, in turn, corresponds to the band-edge energies. Henceforth we shall use the notation k_{edge} to denote the band-edge values of k_z.

As a consequence, it is not hard to see that the system of Eqs. (8a)–(8d), when applied to band-edge energies, allows only solutions with well-defined symmetries (for the same value of k_{edge}): $a=c$ ($a=-c$) and $b=d$ ($b=-d$), in which case the envelope wave functions are even (odd) functions of z.

Second, note that in the limit $h\to\infty$ we recover the "atomic" problem of a particle in a V-shaped well (see Appendix B). Also in this limit, and as a consequence of the symmetry of the triangular potential, the eigenfunctions have definite parity. In particular, the ground state is an even function of z, the first excited state an odd function, etc.

This allows us to conclude that the band-edge wave functions of every odd-index (even-index) subband are even (odd) functions of z in the unit cell.

We will now proceed with the derivation of the eigenvalue equations and envelope wave functions corresponding to the band-edge energies.

A. Odd-index subbands ($n=1,3,5,\ldots$)

The band-edge wave functions corresponding to every odd-index band are even functions of $z(-h/2\le z\le h/2)$. As a consequence, $a=c$ and $b=d$ in Eqs. (5) and (7):

$$\psi^{r}_{nk_{\text{edge}}}(z)=a\ \text{Ai}[-\beta(\alpha-z)]+b\ \text{Bi}[-\beta(\alpha-z)]\ , \tag{12}$$

$$\psi^{l}_{nk_{\text{edge}}}(z)=a\ \text{Ai}[-\beta(\alpha+z)]+b\ \text{Bi}[-\beta(\alpha+z)]\ . \tag{13}$$

Again imposing on wave functions (12) and (13) the boundary conditions of continuity of the wave functions and its derivative at $z=0$ and $h/2$, we obtain three nontrivial equations [the condition of continuity at $z=0$ is satisfied trivially by (12) and (13)],

$$aA'_1+bB'_1=0\ , \tag{14a}$$

$$(1-e^{ik_{\text{edge}}h})(aA_2+bB_2)=0\ , \tag{14b}$$

$$(1+e^{ik_{\text{edge}}h})(aA'_2+bB'_2)=0\ . \tag{14c}$$

The minimum band-edge energy for every odd-index band is obtained particularizing the system (14a)–(14c) for the case $k_{\text{edge}}=0$, in which case (14b) is satisfied trivially, and from (14a) and (14c) we obtain the eigenvalue equation

$$A'_1B'_2-A'_2B'_1=0\ . \tag{15}$$

From (14a) [or (14c)] and the normalization condition in the unit cell,

$$\int_{-h/2}^{h/2}dz\,|\psi^2_{n,k_{\text{edge}}}(z)|^2=1\ , \tag{16}$$

it is not hard to obtain the explicit expression of the coefficient a and the ratio b/a,

$$a=\left[\frac{\pi^2\beta}{2}\frac{(B'_1)^2(B'_2)^2}{\beta(h/2-\alpha)(B'_1)^2+\alpha\beta(B'_2)^2}\right]^{1/2}\ , \tag{17}$$

$$\frac{b}{a}=-\frac{A'_1}{B'_1}\ . \tag{18}$$

Some useful integrals of the Airy functions necessary to get the explicit result (17) can be found in Ref. 20.

Similarly, the maximum band-edge energies for every odd-index band are obtained when the system (14a)–(14c) is particularized to the case $k_{\text{edge}}h=\pm\pi$: (14c) is trivially satisfied, and from (14a) and (14b) we obtain

$$A'_1B_2-A_2B'_1=0\ , \tag{19}$$

while the expressions for the coefficients of the wave function are now

$$a=\left[\frac{\pi^2\beta}{2}\frac{(B'_1)^2B_2^2}{\alpha\beta B_2^2-(B'_1)^2}\right]^{1/2}\ , \tag{20}$$

$$\frac{b}{a}=-\frac{A'_1}{B'_1}\ . \tag{21}$$

B. Even-index subbands ($n=2,4,6,\ldots$)

The band-edge envelope wave functions corresponding to every even-index subband are uneven functions of $z(-h/2\le z\le h/2)$. The general solution given by (5) and (7) reduces to this symmetry when $a=-c$ and $b=-d$:

$$\psi^{r}_{nk_{\text{edge}}}(z)=a\ \text{Ai}[-\beta(\alpha-z)]+b\ \text{Bi}[-\beta(\alpha-z)]\ , \tag{22}$$

$$\psi^{l}_{nk_{\text{edge}}}(z)=-a\ \text{Ai}[-\beta(\alpha+z)]-b\ \text{Bi}[-\beta(\alpha+z)]\ . \tag{23}$$

As before, boundary conditions at $z=0$ and $z=h/2$ produce the following set of equations:

$$aA_1+bB_1=0\ , \tag{24a}$$

$$(1+e^{ik_{\text{edge}}h})(aA_2+bB_2)=0\ , \tag{24b}$$

$$(1-e^{ik_{\text{edge}}h})(aA'_2+bB'_2)=0\ . \tag{24c}$$

However, and unlike the odd-subband case, the minimum band-edge energy for every even-index subband is obtained when $k_{\text{edge}}h=\pm\pi$ in (24a)–(24c). From (24a) and (24c) we obtain the eigenvalue equation

$$A_1B'_2-A'_2B_1=0\ , \tag{25}$$

while from (24a) and the normalization condition (16) the coefficient a and the ratio b/a are

$$a=\left[\frac{\pi^2\beta}{2}\frac{B_1^2(B'_2)^2}{(B'_2)^2-\beta(\alpha-h/2)B_1^2}\right]^{1/2}\ , \tag{26}$$

$$\frac{b}{a}=-\frac{A_1}{B_1}\ . \tag{27}$$

Finally, when $k_{\text{edge}}h=0$ in (24a)–(24c), we obtain the maximum energy for every even-index subband. From (24a) and (24b) we obtain, this time,

$$A_1B_2-A_2B_1=0\ , \tag{28}$$

with the corresponding coefficients for the normalized wave function,

$$a=\left[\frac{\pi^2\beta}{2}\frac{B_1^2B_2^2}{B_2^2-B_1^2}\right]^{1/2}\ , \tag{29}$$

$$\frac{b}{a}=-\frac{A_1}{B_1}\ . \tag{30}$$

Eigenvalue band-edge equations (15), (19), (25), and (28) (and the corresponding expressions for the coefficients) are our desired result. They are simpler than the general result (11), and as a consequence, of easier application.

It should be noted that the band-edge equations are *different* functions (of energy) from the general result (11). They *only* give the same answer (same eigenvalue) for the particular case of band-edge energies. The same applies for the band-edge coefficients with relation to the general coefficients given in Appendix A.

As an example, we will prove the consistency between the general eigenvalue equation (11), when particularized to the minimum band-edge energy of the first subband,

and the corresponding Eq. (15).

Taking into account that $k_z h = 0$ and $A'_1 B'_2 - A'_2 B'_1 = 0$ [Eq. (15)], Eq. (11) reduces to

$$(A_1 B'_2 - A'_2 B_1)(A'_1 B_2 - A_2 B'_1) = -1/\pi^2 . \quad (31)$$

Expanding the left-hand side and again using the eigenvalue equation (15), (31) can be rewritten as

$$(A'_1 B_1 - A_1 B'_1)(A_2 B'_2 - A'_2 B_2) = -1/\pi^2 , \quad (32)$$

which, according to the Wronskian relation satisfied by the Airy functions [Eq. (10)], is an identity. In a quite analogous way, it is possible to check the consistency between (11) and the band-edge expressions (19), (25), and (28).

III. APPLICATION AND DISCUSSION

As an illustration of the application of the expressions obtained in Sec. II, we have calculated the electron, heavy-hole, and light-hole energy subbands as function of the period h and two different values of δ-doping concentration N^{2D}. We have also calculated the corresponding normalized band-edge envelope wave functions for the first two subbands in each case.

The values of the physical parameters we use in the calculations are[21] $m_e^* = 0.067 m_0$, $m_{hh}^* = 0.377 m_0$, $m_{lh} = 0.090 m_0$, and $\epsilon = 12.5$ (m_0 being the free-electron mass).

We show in Fig. 2 the electron, hh, and lh energy subbands as function of h, for a 2D δ-doping concentration $N^{2D} = 12.5 \times 10^{12}$ cm^{-2}. The straight line corresponds to the potential modulation V_0 ($V_0 = eFd/2$). Note that for electrons we have chosen the bottom of the conduction band as the origin of energies, while for the hh's and lh's the origin of energies lies at the top of the valence band.

Most of the experimental studies on sawtooth-doping superlattices have been done for $N^{2D} \simeq 12.5 \times 10^{12}$ cm^{-2} and $h \simeq 150$ Å.[9-12] From the analysis of these experimental results, good agreement has been found between the experimental quantum-confined transitions and theoretical results using the energy levels of a particle in a V-shaped quantum well.

Figure 2 indicates that this analysis, as expected, is justified only for the first two subbands for the electron and lh, while for the hh the first six subbands are in the quantum-well regime.

For comparison, we have repeated the calculations that lead to Fig. 2, but with a concentration of doping impurities 10 times smaller ($N^{2D} = 1.25 \times 10^{12}$ cm^{-2}). The results are shown in Fig. 3. As a consequence of the correspondingly smaller magnitude of the superlattice potential $V(z)$, the bands become much broader for the same period h. For example, for $h \simeq 150$ Å only the first subband corresponding to the hh can be considered in the quantum-well regime, while all the other subbands are in the superlattice regime.

We display in Fig. 4 the band-edge normalized envelope wave functions corresponding to the minimum energy of the first ($n = 1$) electron (solid line), hh (dashed line), and lh (pointed line) subbands for the two values of N^{2D} considered in Figs. 2 and 3.

For this particular case, all wave functions are even in the unit cell (as all the odd-index band-edge wave functions), but are also even from cell to cell.

Note that, as a consequence of the indirect gap in real space characteristic of doping superlattices, the electronic charge distribution is displaced a distance $h/2$ from the hh and lh charge distributions.

The different degrees of localization (for the same N^{2D}) of the electron, heavy holes, and light holes are a direct

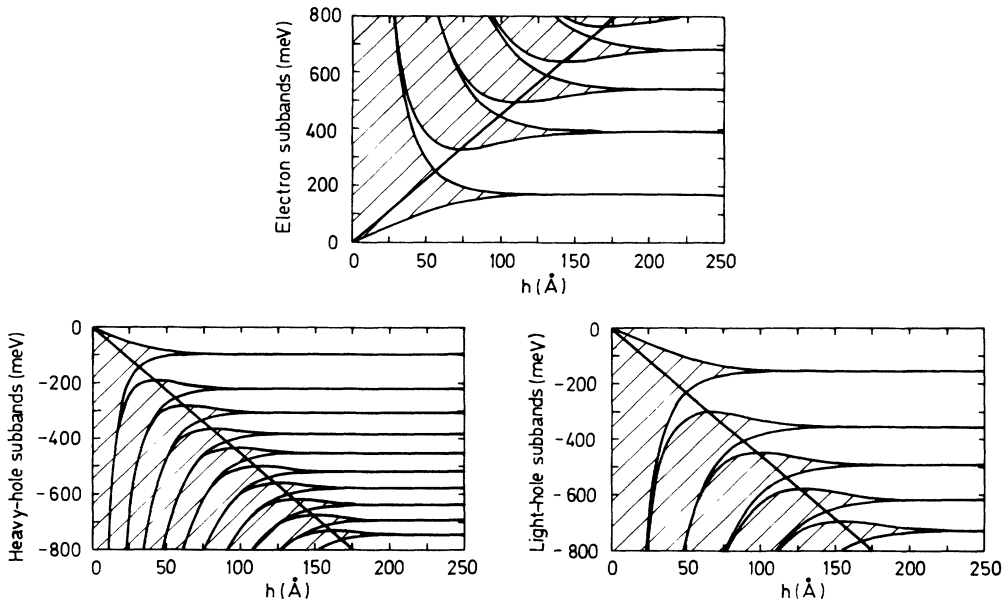

FIG. 2. Calculated subband energies and bandwidths for electrons, heavy holes, and light holes as function of period h. The straight line corresponds to the potential modulation V_0 ($V_0 = eF/2$). $N^{2D} = 12.5 \times 10^{12}$ cm^{-2}.

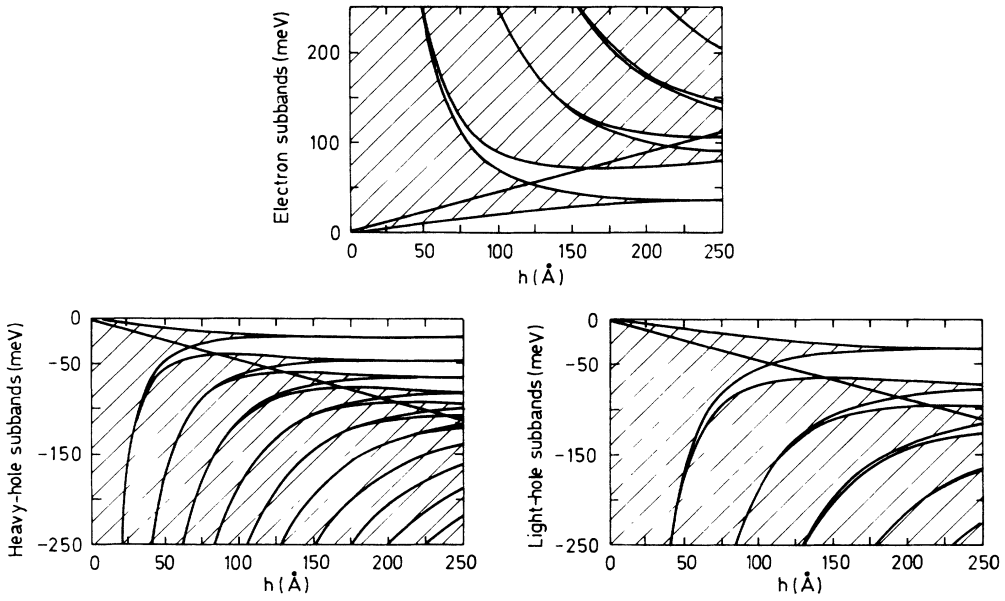

FIG. 3. Calculated subband energies and bandwidths for electrons, heavy holes, and light holes as function of period h. The straight line corresponds to the potential modulation $V_0(V_0=eFd/2)$. $N^{2D}=1.25\times10^{12}$ cm^{-2}.

consequence of their different effective masses ($m_e^* < m_{lh}^* < m_{hh}^*$).

The main difference between Figs. (4a) and (4b) is that the charge distribution is much more uniform in the latter case. It can be seen that, for example, the wave function corresponding to electrons in Fig. 4(b) is essentially a constant with a weak modulation, while in Fig. 4(a) it is essentially concentrated in the well region.

Figure 5 corresponds to the band-edge normalized wave functions associated with the maximum energy of the first ($n=1$) electron, hh, and lh subbands.

The wave functions are even in the unit cell, but they are now odd from cell to cell, unlike the previous case. This means that the wave function (and, consequently, the charge distribution) must be very small in the barrier regions. This condition induces no large changes in the charge distribution when $N^{2D}=12.5\times10^{12}$ [Fig. 5(a)] because the wave function is already very small around such regions. However, when $N^{2D}=1.25\times10^{12}$ cm^{-2} [Fig. 5(b)], the charge distribution moves towards the well regions [cf. Figs. 4(b) and 5(b)]. The overlap between an electron and lh (or hh) wave functions will be larger in the situation of Fig. 4(b) than in that of Fig. 5(b); this, for example, could be an important piece of information in an analysis of experiments of optical absorption in sawtooth-doping superlattices.

We display in Figs. 6 and 7 the band-edge normalized envelope wave functions corresponding to the minimum

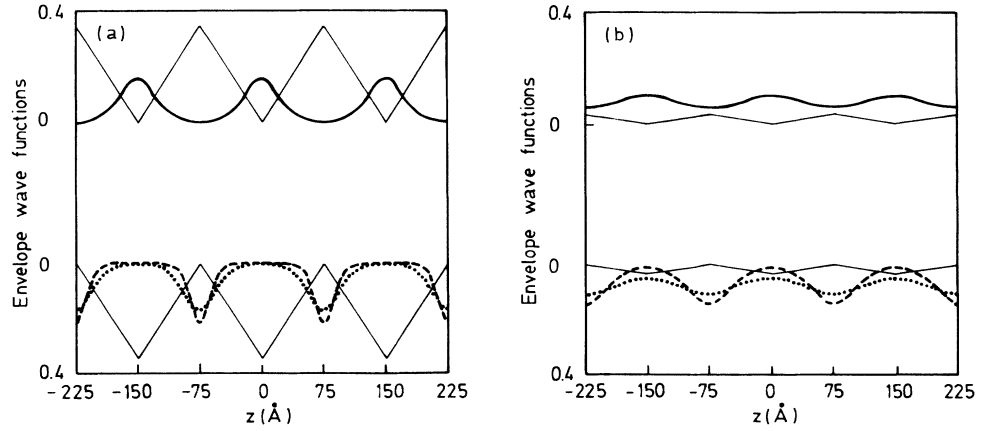

FIG. 4. Band-edge normalized envelope wave functions corresponding to the minimum energy of the $n=1$ subbands. ——, electrons; — — —, hh's; · · ·, lh's. Case (a) corresponds to $N^{2D}=12.5\times10^{12}$ cm^{-2}, while case (b) corresponds to $N^{2D}=1.25\times10^{12}$ cm^{-2}.

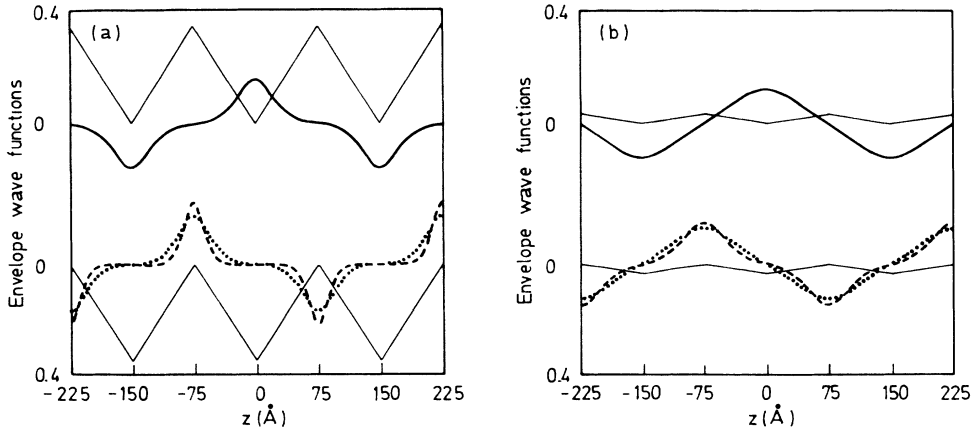

FIG. 5. Band-edge normalized envelope wave functions corresponding to the maximum energy of the $n=1$ subbands. Same convention as in Fig. 4.

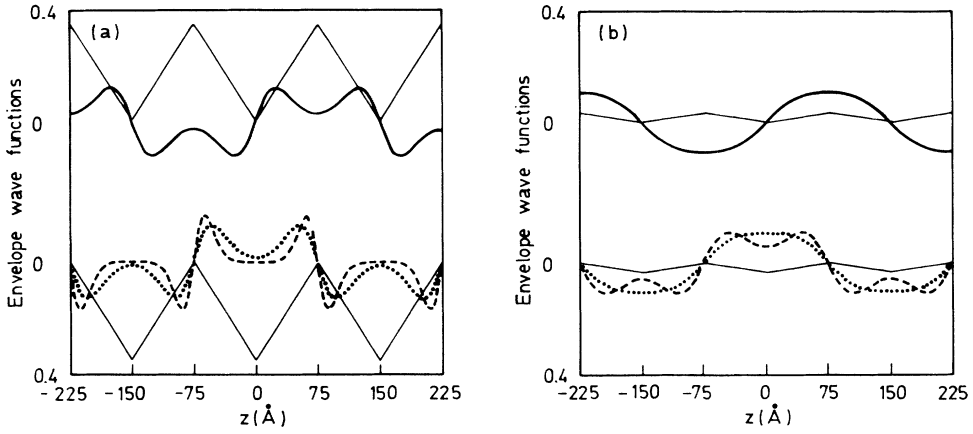

FIG. 6. Band-edge normalized envelope wave functions corresponding to the minimum energy of the $n=2$ subbands. Same convention as in Fig. 4.

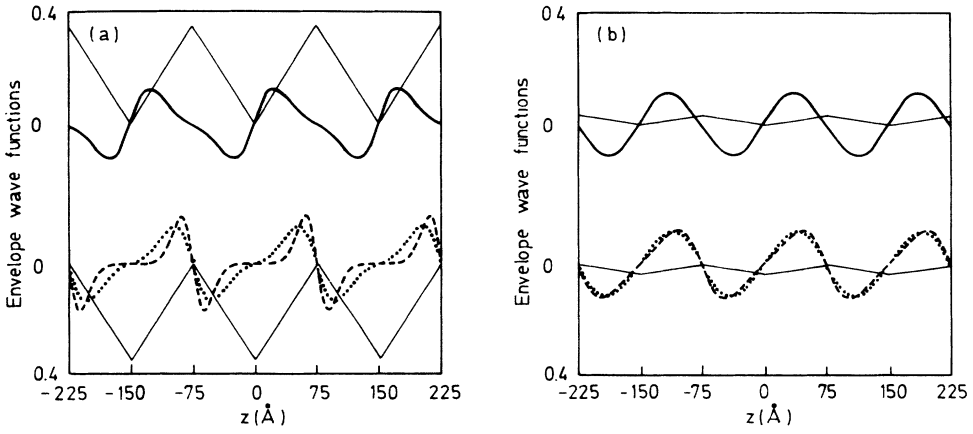

FIG. 7. Band-edge normalized envelope wave functions corresponding to the maximum energy of the $n=2$ subbands. Same convention as in Fig. 4.

and maximum $n=2$ energy subbands, respectively. In both cases the wave functions are odd in the unit cell (as are all the even-index band-edge wave functions), but while in Fig. 6 they are also odd from cell to cell, in Fig. 7 the wave functions are even from cell to cell.

Clearly, as we move towards higher-energy subbands, we approach the "nearly-free-particle" limit,[19] where the periodic potential of the superlattice is a small perturbation compared to the kinetic energy of the particle. For example, the electron envelope wave function of Fig. 7(b) is already very well approximated by $(2/\sqrt{h})\sin(2\pi z/h)$, the band-edge wave function corresponding to a simple nearly-free-particle–limit analysis.

In conclusion, we have calculated the subband energies and charge distribution of a Kronig-Penney model of semiconductor sawtooth-doping superlattices. The analytic expressions obtained become very simple for the particular case of band-edge energies, as a consequence of the definite parity of the envelope wave functions. The results obtained in this work could be very useful for the analysis of this class of superlattices and application to device designs.

APPENDIX A: COEFFICIENTS OF THE NORMALIZED ENVELOPE WAVE FUNCTIONS IN THE GENERAL CASE

From the system of Eqs. (8a)–(8d), the following ratios between the coefficients are readily obtained:

$$\frac{b}{a}=2\pi(KA_1A_1'-A_2A_2')[(1+2\pi A_2'B_2)-K(1+2\pi A_1'B_1)]^{-1}\ , \tag{A1}$$

$$\frac{c}{a}=[B_1B_1'(1+2\pi A_2'B_2)-B_2B_2'(1+2\pi A_1'B_1)](KB_1B_1'-B_2B_2')^{-1}\ , \tag{A2}$$

$$\frac{d}{a}=[(1+2\pi A_1'B_1)-K(1+2\pi A_2'B_2)]\{2\pi[B_2B_2'(1+2\pi A_1'B_1)-B_1B_1'(1+2\pi A_2'B_2)]\}^{-1}\ , \tag{A3}$$

where we have defined $K=e^{ik_zh}$.

Finally, the coefficient a, obtained from the normalization condition of the envelope wave function in the unit cell, is given by

$$a=\left[\frac{\beta}{\mathcal{D}_{\rm I}+\mathcal{D}_{\rm II}+\mathcal{D}_{\rm III}}\right]^{1/2}\ , \tag{A4}$$

where

$$\mathcal{D}_{\rm I}=(1+CC^*)[z_2A_2^2-A_2'^2-z_1A_1^2+(A_1')^2]\ ,$$

$$\mathcal{D}_{\rm II}=(BB^*+DD^*)[z_2B_2^2-(B_2')^2-z_1B_1^2+(B_1')^2]\ ,$$

$$\mathcal{D}_{\rm III}=(B+B^*+CD^*+C^*D)(z_2A_2B_2-A_2'B_2'-z_1A_1B_1+A_1'B_1')\ ,$$

and we have defined $B=b/a$, $C=c/a$, $D=d/a$, $z_1=-\alpha\beta$, and $z_2=-\beta(\alpha-h/2)$.

Replacing (A1) and (A4) in (5), and (A2)–(A4) in (7), gives us the general normalized envelope wave functions, valid for any energy (inside the bands), period, and δ-doping concentration.

It is easy to check that (A1)–(A4) reduces to the simpler expressions given in Sec. II for the special case of band-edge energies.

APPENDIX B: LIMIT $h\to\infty$ OF THE SUPERLATTICE EIGENVALUE EQUATION

An analysis of the limit $h\to\infty$ of (11) is easy and instructive. The asymptotic expansions of the Airy functions are[18]

$$\mathrm{Ai}(x)\simeq\frac{1}{2\sqrt{\pi}}x^{-1/4}e^{-2x^{3/2}/3}\ , \tag{B1}$$

$$\mathrm{Ai}'(x)\simeq\frac{1}{2\sqrt{\pi}}x^{1/4}e^{-2x^{3/2}/3}\ , \tag{B2}$$

$$\mathrm{Bi}(x)\simeq\frac{1}{2\sqrt{\pi}}x^{-1/4}e^{2x^{3/2}/3}\ , \tag{B3}$$

$$\mathrm{Bi}'(x)\simeq\frac{1}{2\sqrt{\pi}}x^{1/4}e^{2x^{3/2}/3}\ . \tag{B4}$$

Replacing A_2, A_2', B_2, and B_2' in (11) by their asymptotic expressions, it is not hard to derive that the eigenvalue equation in the limit $h\to\infty$ reduces to

$$A_1A_1'=0\ , \tag{B5}$$

and consequently the eigenvalues are related to the zeros of A_1 or A_1'.

When $h\to\infty$ the superlattice problem becomes effectively a quantum-well problem of a particle confined to move in a triangular potential. The exact solution of this latter problem coincides with the result (B5).[10,17] In particular, the ground state is even and its energy is related to the first zero of A_1', the first-excited state is odd and its energy is related to the first zero of A_1, etc.

*Permanent address: Instituto de Física, Facultad de Ciencias Exactas y Tecnología, Universidad Nacional de Tucumán, avenida Roca 1800, 4000 San Miguel de Tucumán, Tucumán, Argentina.

[1]L. Esaki and R. Tsu, IBM J. Res. Dev. **14**, 61 (1970).

[2]L. Esaki, in *Proceedings of the 17th International Conference on the Physics of Semiconductors,* edited by J. D. Chadi and W. A. Harrison (Springer-Verlag, San Francisco, 1985).

[3]L. Esaki, IEEE J. Quantum Electron. **QE-22**, 1611 (1986).

[4]D. Mukherji and B. R. Nag, Phys. Rev. B **12**, 4338 (1975).

[5]G. Bastard, Phys. Rev. B **24**, 5693 (1981).

[6]J. N. Schulman and Y. C. Chang, Phys. Rev. B **24**, 4445 (1981).

[7]B. A. Vojak, W. D. Laidig, N. Holoyak, Jr., M. D. Camras, J. J. Coleman, and P. D. Dapkus, J. Appl. Phys. **52**, 621 (1981).

[8]A. Chomette, B. Deveaud, M. Baudet, P. Auvray, and A. Regreny, J. Appl. Phys. **59**, 3835 (1986).

[9]H. Cho and P. R. Prucnal, Phys. Rev. B **36**, 3237 (1987).

[10]E. F. Schubert, B. Ullrich, T. D. Harris, and J. E. Cunningham, Phys. Rev. B **38**, 8305 (1988).

[11]B. Ullrich, C. Zhang, E. F. Schubert, J. E. Cunningham, and K. v. Klitzing, Phys. Rev. B **39**, 3776 (1989).

[12]E. F. Schubert, T. D. Harris, J. E. Cunningham, and W. Jan, Phys. Rev. B **39**, 11 011 (1989).

[13]B. Ullrich, C. Zhang, and K. v. Klitzing, Appl. Phys. Lett. **54**, 1133 (1989).

[14]K. Ploog and G. Döhler, Adv. Phys. **32**, 285 (1983).

[15]E. F. Schubert, J. E. Cunningham, and W. T. Tsang, Phys. Rev. B **36**, 1348 (1987).

[16]G. H. Döhler, Phys. Status Solidi B **52**, 79 (1972); **52**, 533 (1972).

[17]C. R. Proetto, Phys. Rev. B **41**, 6036 (1990).

[18]*Handbook of Mathematical Functions,* edited by M. Abramowitz and I. A. Stegun (U.S. GPO, Washington, D.C., 1964), p. 446.

[19]N. W. Ashcroft and N. D. Mermin, *Solid State Physics* (Holt, Rinehart and Winston, New York, 1976).

[20]F. Stern, Phys. Rev. B **5**, 4891 (1972).

[21]*Physics of Group IV Elements and III-V Compounds, Landölt-Börnstein,* New Series, edited by O. Madelung (Springer, Berlin, 1982), Vol. 17, Pt. a.